AGU PUBLICATIONS

Geophysical Research Letters

RESEARCH LETTER
10.1002/2016GL068061

Key Points:
- We study the frequency dependence of nonlinear elasticity in Berea sandstone
- We find different frequency dependence behavior among the harmonic content
- These findings will ultimately help in better relating the nonlinear elastic behavior to rock microstructure

Supporting Information:
- Supporting Information S1

Correspondence to:
J. Rivière,
jvr5626@psu.edu

Citation:
Rivière, J., L. Pimienta, M. Scuderi, T. Candela, P. Shokouhi, J. Fortin, A. Schubnel, C. Marone, and P. A. Johnson (2016), Frequency, pressure, and strain dependence of nonlinear elasticity in Berea Sandstone, *Geophys. Res. Lett.*, *43*, 3226–3236, doi:10.1002/2016GL068061.

Received 1 FEB 2016
Accepted 18 MAR 2016
Accepted article online 22 MAR 2016
Published online 14 APR 2016

Frequency, pressure, and strain dependence of nonlinear elasticity in Berea Sandstone

Jacques Rivière[1,2], Lucas Pimienta[3], Marco Scuderi[1,4], Thibault Candela[1,5], Parisa Shokouhi[6], Jérôme Fortin[3], Alexandre Schubnel[3], Chris Marone[1], and Paul A. Johnson[2]

[1]Department of Geosciences, Pennsylvania State University, University Park, Pennsylvania, USA, [2]Earth and Environmental Sciences, Los Alamos National Laboratory, Los Alamos, New Mexico, USA, [3]École Normale Supérieure (ENS), Laboratoire de Géologie, Paris, France, [4]Department of Earth Sciences, La Sapienza Universit di Rome, Rome, Italy, [5]TNO, Geological Survey of The Netherlands, TA Utrecht, Netherlands, [6]Department of Civil Engineering, Pennsylvania State University, University Park, Pennsylvania, USA

Abstract Acoustoelasticity measurements in a sample of room dry Berea sandstone are conducted at various loading frequencies to explore the transition between the quasi-static ($f \to 0$) and dynamic (few kilohertz) nonlinear elastic response. We carry out these measurements at multiple confining pressures and perform a multivariate regression analysis to quantify the dependence of the harmonic content on strain amplitude, frequency, and pressure. The modulus softening (equivalent to the harmonic at 0f) increases by a factor 2–3 over 3 orders of magnitude increase in frequency. Harmonics at 2f, 4f, and 6f exhibit similar behaviors. In contrast, the harmonic at 1f appears frequency independent. This result corroborates previous studies showing that the nonlinear elasticity of rocks can be described with a minimum of two physical mechanisms. This study provides quantitative data that describes the rate dependency of nonlinear elasticity. These findings can be used to improve theories relating the macroscopic elastic response to microstructural features.

1. Introduction

The main motivation of this study is to improve our understanding of nonlinear elastic properties of rocks, in particular frequency (-time) and pressure dependences. In terms of modeling, one wants to improve theoretical descriptions that relate nonlinear measures to microstructural properties of rocks [*Guyer and Johnson*, 2009]. Nonlinear elasticity is relevant for a broad range of applications in geosciences, including earthquake slip processes, strong ground motion [*Beresnev and Wen*, 1996; *Field et al.*, 1997; *Renaud et al.*, 2014; *Trifunac and Todorovska*, 1996], liquefaction phenomenon [*Aguirre and Irikura*, 1997], Earth tides [*Hillers et al.*, 2015], and oil/gas exploration. Further, a better knowledge of frequency dependence facilitates comparisons between observations made at different scales, e.g., from the laboratory to the field scale.

A number of studies [*Winkler and Liu*, 1996; *Winkler and McGowan*, 2004] have characterized nonlinear elasticity of rocks using acoustoelastic experiments. Such experiments consists in measuring speed of sound with high-frequency (HF) pulses across the sample while it is gradually stressed uniaxially and/or hydrostatically at increasing levels. These quasi-static acoustoelastic experiments are equivalent to zero-frequency measurements. In dynamic acoustoelastic testing (DAET), the stepwise increases in pressure/stress are replaced by a low-frequency (LF) strain modulation [*Renaud et al.*, 2011]. DAET is therefore a pump-probe scheme in which the HF elastic pulses probe the state of a mechanical system set by the LF wave, the pump. For the pump P we often use the fundamental compressional mode of the sample driven to strain amplitudes $10^{-7} \leq \epsilon_P < 10^{-5}$ ($\epsilon_P \equiv \epsilon$ hereafter) [*Renaud et al.*, 2011]. The probe (p) is a HF pulse (of low strain amplitude, $\epsilon_p \simeq 10^{-7}$) that tests the state of the sample at all phases of the pump strain field, i.e., in both compression and tension. From the response of the probe to the pump modulation, a complete description of the rich nonlinear elastic properties of the sample is obtained, e.g., hysteresis, tension/compression asymmetry, and nonlinear elastic constants, providing a more complete picture on the nonlinear phenomena than static experiments [*Renaud et al.*, 2009, 2010, 2011, 2013a, 2013b, 2014; *Moreschi et al.*, 2011; *Trarieux et al.*, 2014; *Rivière et al.*, 2013, 2015].

One objective of this study is to investigate the transition between quasi-static (frequency $f_P \to 0$, $f_P \equiv f$ hereafter) and dynamic acoustoelasticity ($f \simeq$ few kilohertz). To explore such transition, the experimental

setup is similar to quasi-static experimental setups, except that the mechanical press will oscillate the sample sinusoidally at frequencies ranging from 0.2 up to 250 Hz, instead of applying stepwise increase in stress. A second objective is to quantify the effect of confining pressure on the dynamic nonlinear parameters. This is especially important when nonlinear properties of rocks under natural in situ conditions are concerned.

The organization of the paper is as follows. In section 2, we describe the apparatus, the test protocol, and the data analysis. In section 3, we describe the experimental results, before discussing them in section 4.

2. Experiment

The test sample is a cylinder of room dry Berea sandstone of length $L = 8$ cm and diameter $d = 4$ cm (Figure 1a). The experiments are conducted in an oil-confining triaxial apparatus [*Fortin et al.*, 2005]. The sample is radially enclosed in a rubber jacket in order to be separated from the oil-confining medium. The apparatus has been developed and calibrated to measure LF Young modulus and Poisson ratio from axial oscillations at low strain amplitudes [*Pimienta et al.*, 2015a, 2015b]. The LF axial stress oscillations are exerted using a Physik Instrumente (PI) piezoelectric actuator (Figures 1a and 1b). The LF sample's strain oscillations are recorded using two pairs of axial and radial FCB 350 Ω strain gauges from TML (Tokyo Sokki). HF longitudinal wave velocity is measured from a pair of *P* wave piezoelectric sensors glued radially on the perimeter of the sample (Figure 1a). We ensure that the ultrasonic time of flight t^0 across the sample (for a longitudinal wave velocity c_0 in Berea, $t^0 = d/c_0 = 0.04/2700 \simeq 15$ μs, Figure 1c) is much shorter than the pump period $T = 1/f = 1/250 = 5$ ms, even at the largest pump frequency (250 Hz). This condition is required to make certain that the strain induced by the pump changes very little during each ultrasonic propagation.

The signals measured by the strain gauges are recorded using a Catman system from HBM Inc. (LF device). The sampling rate is 50 Hz for $f \leq 2$ Hz, 400 Hz for $2 < f \leq 20$ Hz, and 2.4 kHz for $f > 20$ Hz. The ultrasonic source signal is three periods of 500 kHz broadcast. The ultrasonic detection is sampled at 50 MHz on a separate data acquisition system (HF device). To synchronize the pump and the probe broadcasts, the HF device simultaneously records the input signal of the piezoelectric actuator used for the pump oscillations.

The measurement protocol involves the following steps. At time $t = t_0 = 0$, the ultrasonic source is turned on, sending 500 kHz pulses at a sequence of times $t_j, j = 1, 2, \ldots$. The time between successive pulses, ΔT, is chosen such that the coda received in response to the jth pulse decays to zero before sending the $(j+1)$th pulse. Due to the limited onboard memory of the acquisition card, we use different ΔT depending on the pump frequency, ranging from 1 ms (at $f = 250$ Hz) up to 50 ms for $f = 0.1$ Hz. A full acquisition always therefore consists of 3000 ultrasonic pulses, independent of pump frequency. The piezoelectric actuator, at frequency f and amplitude A, is turned on after the broadcast of a minimum of 10 ultrasonic pulses (Figure 1b), to properly estimate the speed of sound across the sample in the absence of pump oscillations. The subsequent HF pulses are launched in the presence of pump oscillations.

We record such acquisitions for pump frequency f varying from 0.2 to 250 Hz, pump strain amplitudes ϵ varying from 9×10^{-7} to 2×10^{-5} and confining pressures P_c varying from 0.1 (ambient) to 30 MPa.

2.1. Data Analysis

The LF measurements rely on the stress-strain method [e.g., *Batzle et al.*, 2006]. An axial stress oscillation σ_{ax} of a given frequency is applied, inducing axial ϵ_{ax} and radial ϵ_{rad} strain oscillations of the rock sample. Examples of typical stress-strain curves are reported in Figure S1 in the supporting information. The pump strain amplitude ϵ is determined by collecting the maximum axial strain reached during the oscillation. The LF elastic properties can be deduced from linear regressions (i) between σ_{ax} and ϵ_{ax} to obtain Young modulus E, and (ii) between ϵ_{rad} and ϵ_{ax} to obtain Poisson ratio ν. Young modulus is found to increase from about 25 GPa at ambient pressure to 40 GPa at $P_c = 30$ MPa, while Poisson ratio increases from 0.1 to 0.14. Because the primary goal of the paper is to focus on acoustoelasticity and its frequency, amplitude, and pressure dependences, no further analysis on the elastic moduli is reported here.

Each pulse $s(t - t_j)$ propagating during the pump oscillation is compared to a reference pulse that crosses the sample before the piezoelectric actuator is turned on, e.g., $s(t - t_0)$. The time between successive pulses, ΔT, is chosen to be incommensurate with $T = 1/f$ so that over time the ultrasonic broadcasts at times $\{t_j\}$ sample all phases of the pump strain field.

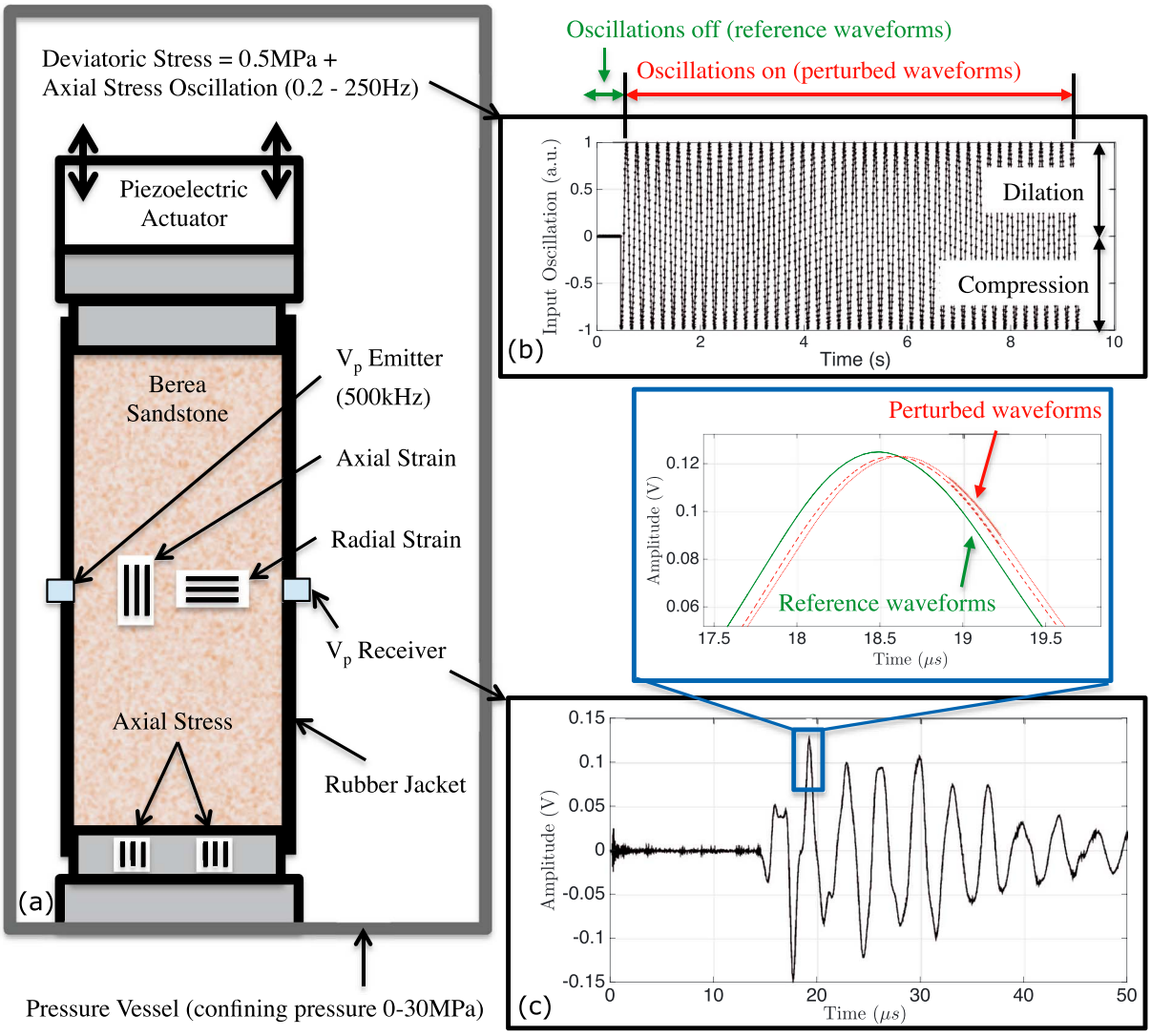

Figure 1. Experimental setup and protocol. (a) The sample is placed inside a pressure vessel where the confining pressure P is increased from ambient up to 30 MPa. The piezoelectric actuator on top oscillates the sample around a constant deviatoric stress of 0.5 MPa at frequencies ranging from 0.2 up to 250 kHz and strain amplitudes roughly from 1 to 10 microstrains. Axial and radial strains (respectively stresses) are measured with strain gauges placed on the sample (respectively on the aluminum base). One pair of piezoceramics is glued on the perimeter of the sample to send/receive longitudinal ultrasonic waves. They launch high-frequency pulses centered at 500 kHz to probe the sample at a given strain level established by the oscillations. (b) Typical oscillations protocol applied to the sample (here at 5 Hz). No oscillations are applied during 0.5 s to serve as a reference for ultrasonic waveforms. (c) Typical received ultrasonic waveform. The inset (blue) shows that waveforms received during oscillations are slightly delayed (and of lower amplitude) than reference waveforms.

The first step in analysis of $s(t - t_j)$ from the steady state time domain is to compare it to the reference pulse $s(t - t_0)$ by computing the cross correlation:

$$C(\tau, t_j) = \int_0^\infty s(t - t_0)s(t + \tau - t_j)\mathrm{d}t \tag{1}$$

to determine $\tau_{\max}(t_j)$, the time τ at which the correlation function is maximum [*Renaud et al.*, 2009, 2010]. This time of flight shift can be converted into a relative velocity change using

$$\frac{\Delta c}{c}(t_j) = -\frac{\tau_{\max}(t_j)}{t^0}, \tag{2}$$

where t^0 is the time of flight of the reference pulse. An example of $\Delta c/c$ curves (variations over the course of one acquisition) is depicted in Figure 2. In Figure 2a, one can see the pump oscillation applied to the sample. In this example, the oscillations start approximately half a second after launching the ultrasonic pulses. As shown

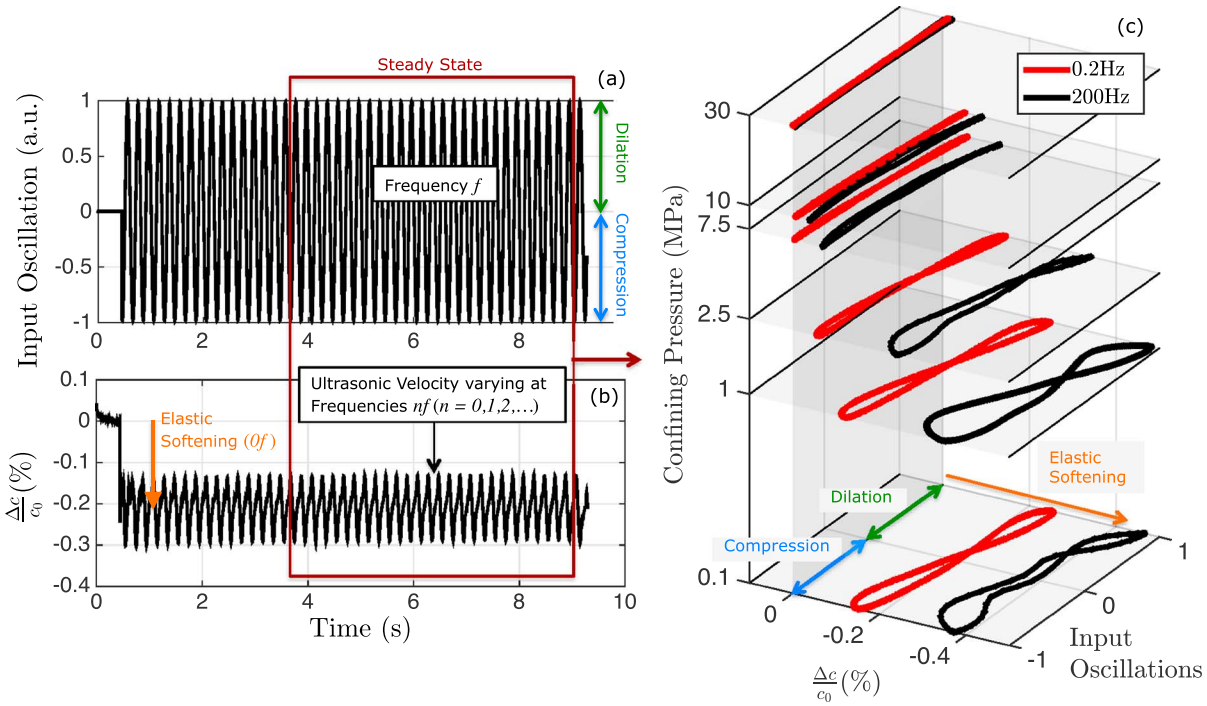

Figure 2. Change in ultrasonic velocity during pump oscillations. (a) Input oscillations of the piezoelectric actuator. Positive (negative) values corresponds to the dilation (compression) phase. In this example, the oscillation frequency is 5 Hz and the output axial strain amplitude is roughly 10 microstrains. (b) Relative change in ultrasonic velocity (see equation (2)) induced by pump oscillations and varying at frequencies nf with $n = 0, 1, 2, \ldots$. The steady state regime is further decomposed applying Fourier analysis. The component at $0f$ corresponds to an elastic softening of the medium. (c) Instantaneous velocity change during steady state at two extreme frequencies (0.2 Hz and 200 Hz) and different confining pressures. One can see a larger change in velocity (i.e., larger nonlinearity) at high frequencies and low confining pressures.

in Figure 2b, the velocity remains constant (i.e., $\frac{\Delta c}{c} = 0$) until the pump is turned on. As soon as the pump is on, the velocity drops and starts oscillating with the pump frequency f, as well as with multiples of f. The velocity drop, or offset, corresponds to an elastic softening of the medium and can be considered as a *zero-frequency* harmonic ($0f$). The three terms (offset, elastic softening, and $0f$ component) will be used interchangeably throughout the document. We perform a dedicated Fourier analysis analogous to a lock-in amplifier [*Rivière et al.*, 2013, 2015] to each $\Delta c/c$ signal to extract the amplitude of the harmonics. These amplitudes are referred to as $\frac{\Delta c}{c}|_{nf}$ with $n = 0, 1, 2, \ldots$. It is worth noting that even components ($0f, 2f, 4f$, and $6f$) for such pump-probe scheme are equivalent to *odd* harmonics (fundamental at frequency f, third, fifth, and seventh harmonics) in standard nonlinear acoustic techniques [*Buck et al.*, 1978; *Van Den Abeele et al.*, 2000], i.e., when the probing wave also acts as a pump. Similarly, the component at $1f$ here is equivalent to the second harmonic in standard techniques.

3. Results

Figure 2c shows the instantaneous change in velocity $\left(\frac{\Delta c}{c}\right)$ as a function of the LF input oscillations. These *nonlinear signatures* closely resemble the ones in *Renaud et al.* [2013b] and *Rivière et al.* [2015] obtained at few kilohertz and ambient pressure. The signatures are complex at low pressure with the presence of hysteresis and elastic softening, roughly 0.5% drop in velocity, which corresponds to a 1% drop in elastic modulus M (assuming a constant density ρ, $\frac{\Delta M}{M} = 2\frac{\Delta c}{c} \simeq 1\%$ with $M = \rho c^2$). Elastic softening as well as hysteresis becomes smaller and smaller with increasing pressure. At 30 MPa, the nonlinearity (offset and hysteresis) approaches toward zero; the two curves overlapping almost completely on the linear vertical plan $\left(\frac{\Delta c}{c} = 0\right)$. Finally, both the offset and hysteresis are larger at 200 Hz than at 0.2 Hz.

We study the dependence of harmonic amplitudes $\left(\frac{\Delta c}{c}\Big|_{nf} \text{ with } n = 0, 1, 2, \ldots\right)$ as a function of frequency, pressure and strain amplitude (Figure 3) obtained through Fourier analysis of each $\Delta c/c$ signal. Figure 3a shows the frequency dependence at three confining pressures and constant pump strain amplitude

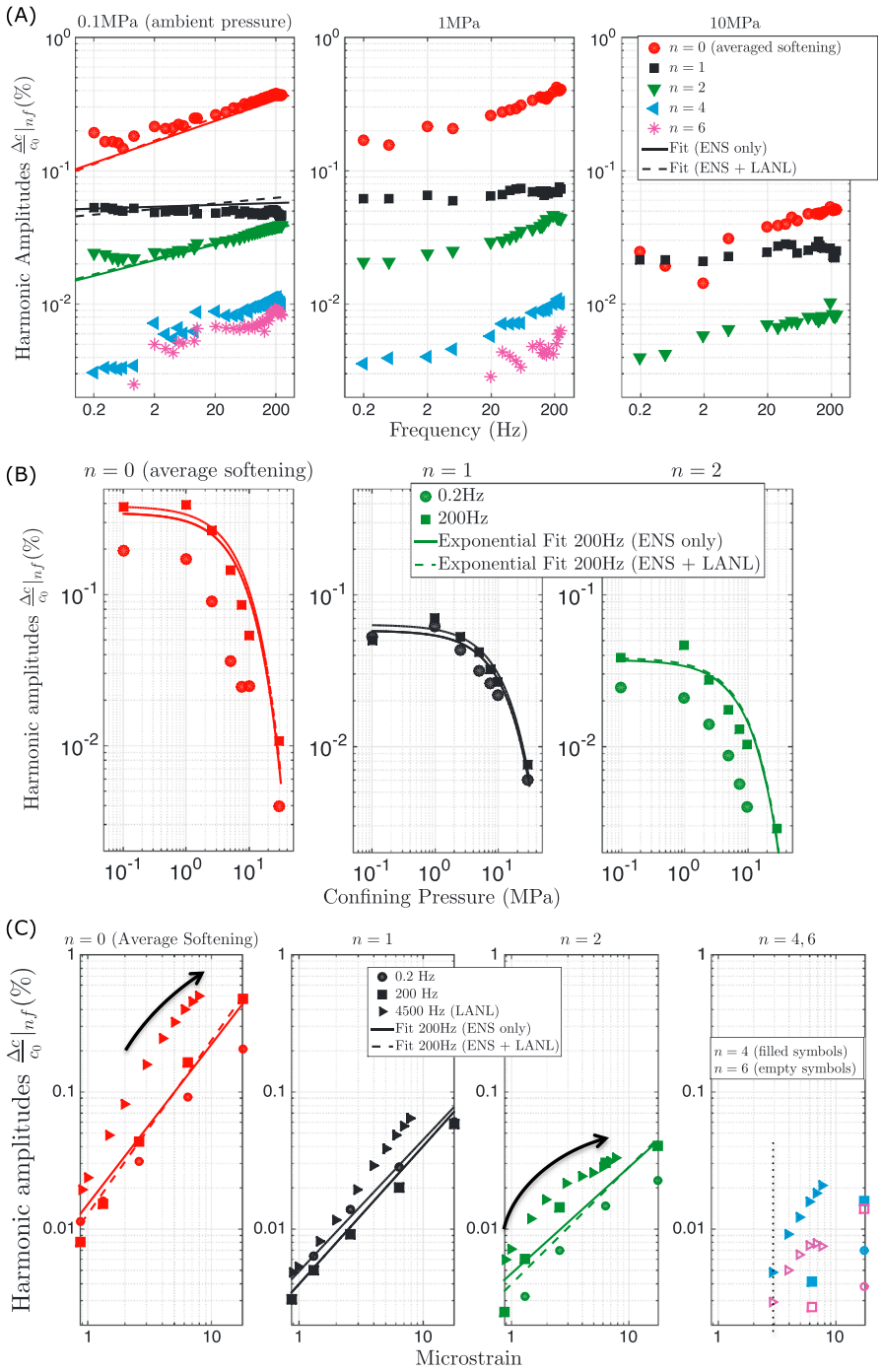

Figure 3. Frequency, pressure, and strain dependences of the harmonic amplitudes. Note that the harmonic amplitudes $\frac{\Delta c}{c}\Big|_{nf, n\geq 1}$ are positive by definition (result of Fourier analysis). On the other hand, because the component at 0*f* corresponds to an elastic softening of the medium (therefore negative), $-\frac{\Delta c}{c}\Big|_{0f}$ is actually represented in the log plot. (a) Pump frequency dependence of the harmonic amplitudes at three confining pressures and constant strain amplitude ($\epsilon \simeq 14$ microstrains). One sees an increase in nonlinearity by a factor 2–3 over three orders of magnitude in frequency for all harmonics but the component at 1*f* and at all pressures. Result of the multivariate regression is also shown at ambient pressure. (B) Pressure dependence at 0.2 and 200 Hz and constant strain amplitude ($\epsilon \simeq 14$ microstrains). Result of the multivariate regression for data at 200 Hz shows the approximate exponential decrease of nonlinearity with confining pressure. (c) Strain dependence at 0.2 Hz, 200 Hz (ENS data), and 4500 Hz (LANL data) at ambient pressure. Result of the multivariate regression for data at 200 Hz show the power law dependence of nonlinearity with strain. The arrows show changes in dependence occurring at strains where higher harmonics at 4*f* and 6*f* emerge from noise (vertical dashed line). Strain dependence at larger pressures is presented in Figure S3 in the supporting information.

($\epsilon \simeq 1.4\times10^{-5}$). The harmonic content at $0f$, $2f$, $4f$, and $6f$ (equivalent to odd harmonics in standard nonlinear techniques [*Buck et al.*, 1978; *Van Den Abeele et al.*, 2000]) increases by a factor 2 or 3 over 3 orders of magnitude in frequency, whereas $\frac{\Delta c}{c}\Big|_{1f}$ (equivalent to the second harmonic in standard nonlinear techniques) seems to be rather invariant. Components at $3f$ and $5f$ are below the noise level. All harmonics are decreasing with increasing confining pressure. In particular, components at $4f$ and $6f$ become progressively unmeasurable with increasing pressure.

In Figure 3b, we focus on the pressure dependence of the first three harmonics ($n = 0, 1, 2$) at two extreme frequencies ($f = 0.2$ and 200 Hz). The nonlinearity decreases by more than an order of magnitude when pressure increases from 1 to 30 MPa, following an approximate exponential decrease. At 30 MPa, the harmonic amplitudes still persist, suggesting that small nonlinearity might still be present at such pressures and potentially measurable if one further reduces noise level of the experimental setup. In addition, as seen in Figure 3a, the nonlinearity is larger at 200 Hz than at 0.2 Hz for components at $0f$ and $2f$, whereas it is similar for the component at $1f$.

Figure 3c shows the strain dependence of the harmonic amplitudes at two extreme frequencies (0.2 and 200 Hz) and ambient pressure. Data from *Rivière et al.* [2015] obtained at $f = 4500$ Hz and ambient pressure are also presented for comparison. The strain dependence found at 0.2 and 200 Hz is similar to that previously found at 4500 Hz [*Rivière et al.*, 2013, 2015].

The component at $0f$ (elastic softening) exhibits a power law behavior ranging between 1 (linear) and 2 (quadratic). The component $\frac{\Delta c}{c}\Big|_{1f}$ evolves linearly with strain. As for $\frac{\Delta c}{c}\Big|_{2f}$, the power law behavior is not constant over the strain range considered. It evolves progressively from a slope larger than 1 at lower strains to a slope less than 1 at higher strains. Finally, one sees higher harmonics at $4f$ and $6f$ emerging from noise at large strains. The larger the frequency, the lower the strain at which they emerge: 3 microstrains at 4500 Hz, 6 microstrains at 200 Hz, and 11 microstrains at 0.2 Hz.

We perform a multivariate regression analysis to quantify the dependence of the harmonic amplitudes on strain, frequency, and confining pressure and highlight main differences among them. To this end, we use a simple linear model of $\log\left(\frac{\Delta c}{c}\Big|_{nf}\right)$ $n = 0, 1, 2$ with variables P, $\log(f)$ and $\log(\epsilon)$. In developing the regression model, in addition to the data presented above (thereafter called *ENS* data), we also include the set of data collected at $f = 4500$ Hz [*Rivière et al.*, 2013, 2015] (thereafter called *LANL* data and shown in Figure 3c). This data set was collected on a different sample taken from the same block of rock as the one used for ENS measurements. The details of LANL setup is described in *Rivière et al.* [2013] and *Rivière et al.* [2015]. LANL data set was taken at ambient pressure and room dry conditions. The full data set is composed of 267 measurements corresponding to different combinations of frequency, pressure, and strain. The multivariate regression analysis is most effective when we start with reasonable assumptions concerning dependence of the predicted variable $\left(\log\left(\frac{\Delta c}{c}\Big|_{nf}\right)\right)$ on the predictors (f, P, and ϵ). The experimental observations shown in Figure 3a suggest that a power law relation between harmonic amplitudes and frequency is appropriate:

$$\frac{\Delta c}{c}\Big|_{nf} = \Phi_1 f^{\mu}. \tag{3}$$

Applying a log transformation to this equation, we obtain the following linear relation between $\log\left(\frac{\Delta c}{c}\Big|_{nf}\right)$ and $\log(f)$:

$$\log\left(\frac{\Delta c}{c}\Big|_{nf}\right) = \mu \log(f) + \log(\Phi_1). \tag{4}$$

For pressure, Figure 3b suggests that the nonlinearity decreases exponentially with confining pressure:

$$\frac{\Delta c}{c}\Big|_{nf} = \Phi_2 e^{-\frac{P}{P_0}}, \tag{5}$$

where P_0 represents a characteristic pressure, which might differ for the different harmonics. Applying a log transformation to this equation yields to the following linear relation:

$$\log\left(\frac{\Delta c}{c}\Big|_{nf}\right) = -\frac{1}{P_0 \ln(10)} P + \log(\Phi_2), \tag{6}$$

Table 1. Coefficients Found From the Multivariate Regression Analysis When Considering ENS Data Only, Based on Equation (9)[a]

	Coefficient	$n = 0$	$n = 1$	$n = 2$
	Constant	2.8297 (3.3152)	1.6070 (1.3584)	0.0453 (0.4330)
Strain ϵ	ν	1.1675 (1.2670)	1.0071 (0.9610)	0.7735 (0.8512)
Frequency f	μ	0.1575 (0.1754)	0.0140 (0.0422)	0.1174 (0.1180)
Pressure P	P_0	7.6730 (7.6730)	13.4042 (13.4042)	10.7499 (10.7499)
r^2		0.9154 (0.9153)	0.9670 (0.9650)	0.9137 (0.9111)

[a]Values in parentheses correspond to coefficients found when considering both ENS and LANL data (taken at 4500 Hz and ambient pressure). The adjusted coefficients of determination r^2 are also provided for both cases, showing the overall appropriate fit.

Finally, power law relations best describe the strain dependence [*Scalerandi et al.*, 2015; *Bruno et al.*, 2009; *Rivière et al.*, 2015], as observed in Figure 3c:

$$\left.\frac{\Delta c}{c}\right|_{nf} = \Phi_3 \epsilon^{\nu}, \tag{7}$$

or equivalently

$$\log\left(\left.\frac{\Delta c}{c}\right|_{nf}\right) = \nu \log(\epsilon) + \log(\Phi_3), \tag{8}$$

Using equations (4), (6), and (8), our linear multivariate model will therefore be

$$\log\left(\left.\frac{\Delta c}{c}\right|_{nf}\right) = \mu \log(f) - \frac{1}{P_0 \ln(10)} P + \nu \log(\epsilon) + \text{Cte}. \tag{9}$$

The linear regression model when fitted to ENS data yields the adjusted coefficients of determination r^2 of 0.9154, 0.9670, and 0.9137 for predicting $\log\left(\left.\frac{\Delta c}{c}\right|_{nf}\right)$ for $n = 0$, $n = 1$, and $n = 2$, respectively. Coefficients are displayed in Table 1. Adding the LANL data set slightly changes the values of the coefficients of determination r^2 (0.9153, 0.9650, and 0.9111) and regression (coefficients in parentheses in Table 1). Regression results displayed in Figure 3 show that these simple models for pressure, strain, and frequency dependences provide an overall appropriate fit for the data set.

From Table 1, we see that the dependence in frequency for $n = 1$ (0.0140) is an order of magnitude lower than for $n = 0$ (0.1575) and $n = 2$ (0.1174), which confirms observations made in Figure 3a (frequency dependence for $n = 0, 2$; frequency independence for $n = 1$). Characteristic pressures for the three harmonics are found to be about 7.7, 13.4, and 10.7 MPa for $n = 0$, 1 and 2, respectively. For strain dependence, one sees that the coefficients for $n = 1$ is very close to one, as found for various other samples in *Rivière et al.* [2015]. For the offset ($n = 0$), ν is found larger than 1 (1.27 in Table 1), which is consistent with former results [*Rivière et al.*, 2013, 2015] where the dependence evolves from quadratic ($\nu = 2$) at low strain to linear at large strains ($\nu = 1$). For the curvature ($n = 2$), ν is found lower than 1 (0.85 in Table 1), which is again consistent with *Rivière et al.* [2015]) for strains larger than a microstrain.

4. Discussion

4.1. Frequency (Strain Rate) Dependence

The increase in nonlinearity with frequency/strain rate (Figure 3a) is consistent with first observations made with resonance and quasi-static methods [*TenCate and Shankland*, 1996; *TenCate*, 2011]. A previous study [*Rivière et al.*, 2015] also suggested that the amplitude dependences of a set of disparate rocks could be explained by a minimum of two different nonlinear mechanisms, one related to the $1f$ component and the second one related to components at $0f$, $2f$, $4f$, and $6f$. Our results regarding frequency dependence also confirm this separation in two mechanisms. The first one, controlling the harmonic at $1f$, appears to be frequency independent, whereas the second one, controlling the harmonics at $0f$ and $2f$, depends on frequency and/or strain rate amplitude, i.e., how quickly the sample is brought from one state to another.

We observe in Figure 2c—as well as in previous references, e.g., *Renaud et al.* [2013b, 2015]—that nonlinear signatures do not exhibit abrupt jumps at extreme strains, i.e., the hysteresis in stress-strain diagrams does

not exhibit any cusps. This observation is in contradiction with numerous quasi-static observations [*TenCate*, 2011; *Guyer et al.*, 1997]. This discrepancy is not fully understood, but we believe that the cusps observed in quasi-static experiments arise due to the combined effects of (i) a lack of precision in measuring small stress and strain with standard mechanical test machines and (ii) the triangular protocols used to perform such tests, implying an instantaneous change in strain rate at each extrema. In contrast, our setup involves a sinusoidal protocol (sinusoidal pump at frequency f) and is made of an additional ultrasonic probe that enables the detection of very fine changes in elasticity. Phenomenological models based on a Presaich-Mayergoyz distribution of hysterons [*McCall and Guyer*, 1994; *Van Den Abeele et al.*, 1997] lead to a stress-strain relation which depends on the sign of the strain rate, leading to cusps in the stress-strain diagram. Other physical models based on friction and/or adhesion processes [*Lawn and Marshall*, 1998; *Nihei et al.*, 2000; *Aleshin and Van Den Abeele*, 2007a; *Tutuncu et al.*, 1998; *Aleshin and Van Den Abeele*, 2007b; *Lebedev and Ostrovsky*, 2014] also lead to cusps in the stress-strain curves. Our results exhibiting (i) no jump in modulus/velocity versus strain diagrams and (ii) an increase in nonlinearity with frequency suggest that models with rate/time dependencies better describe nonlinear elastic phenomena in rocks. Models found in *Vakhnenko et al.* [2005], *Gliozzi and Scalerandi* [2014], *Pecorari* [2015], *Gusev and Tournat* [2005], and *Favrie et al.* [2015] include (or lead to) such rate dependence.

4.2. Pressure Dependence

Nonlinearity decreases by an order of magnitude over the pressure range (0–10 MPa), as found in an earlier study [*Zinszner et al.*, 1997]. The exponential model chosen in equation (5) seems appropriate to describe the pressure dependence of nonlinearity (Figure 3b). This exponential dependence is also observed in the literature for other physical properties like resistivity [*Brace et al.*, 1968; *Kaselow and Shapiro*, 2004], compressibility [*Zimmerman et al.*, 1986], permeability [*Brace et al.*, 1968; *Ougier-Simonin et al.*, 2011; *Wang et al.*, 2013], and wave speeds [*Sayers*, 2002; *Kaselow and Shapiro*, 2004; *Wang et al.*, 2013], with similar characteristic pressures (∼10 MPa, as seen in Table 1). It is generally attributed to crack closure leading to a reduction of pore space connectivity. Observing similar dependences in Figure 3b suggests that crack closure is the main source of nonlinearity within this Berea sample. It is worth noting that characteristic pressures are of the same order of magnitude for all nonlinear components (∼10 MPa). This could indicate that the two aforementioned phenomena (one related to $1f$, the other to $0f, 2f, \ldots$) are both related to crack closure. Although the underlying microstructural mechanisms remain unknown, adhesion forces at grain boundaries are often cited as a possible source of nonlinearity [*Lebedev and Ostrovsky*, 2014]. In particular, the low-amplitude dynamic shaking would disturb the surface forces leading to a transient elastic weakening ($0f$ component). These adhesion effects would become negligible as confining pressure is increased and cracks closed.

It is also worth noting that wave speed (c_0) versus pressure (P_c) measurements mentioned above [*Sayers*, 2002; *Kaselow and Shapiro*, 2004; *Wang et al.*, 2013] are directly related to nonlinear properties since the derivative $\frac{dc_0}{dP_c}$ is a quasi-static equivalent to the $1f$ component, as measured in quasi-static acoustoelasticity [*Winkler and Liu*, 1996; *Winkler and McGowan*, 2004]. From our data set, we can deduce $c_0 = d/t^0$ at all pressures from the reference waveforms (before any oscillations are applied), where t^0 is a reference time of flight as defined in equation (2). We find that the increase in c_0 with pressure can be fitted with a exponential function (Figure S2 in the supporting information) with a characteristic pressure 6.9 MPa similar to the ones found in Table 1. Since $\frac{d}{dx}(e^x) = e^x$, nonlinearity deduced from this quasi-static measurement also evolves as a exponential, which is consistent with the exponential decrease of the $1f$ component.

4.3. Amplitude Dependence

Small arrows in Figure 3c indicate that strain dependence is not constant over the entire strain range, especially for the $2f$ component. One also sees that this change in scaling arise at strains where higher harmonics ($4f$–$6f$) emerge from the noise level, which suggests that both effects are related. The physical mechanism behind this phenomena is still unclear. It might arise from clapping phenomena of the weak contacts within microstructure, as observed in granular assemblies of glass beads [*Tournat et al.*, 2008], leading to an energy transfer from $0f$ and $2f$ components to higher harmonics ($4f$ and $6f$). Further at higher pressure (see Figure S3 in the supporting information), neither changes in strain dependence nor higher harmonics are observed, due to progressive crack locking and closure with pressure. Finally, and as previously observed in *Rivière et al.* [2015], the change in dependence is only present for $0f$ and $2f$ components (i.e., not for $1f$), indicating that the origin of nonlinear elastic phenomena arise from two main mechanisms.

4.4. At Larger Scales

The relative small change in response (factor 2 or 3 over 3 orders of magnitude in frequency) suggests that phenomena observed at the laboratory scale with acoustic experiments (kHz range) are likely to occur in the Earth at seismic frequencies. For instance, a previous in situ study [*Renaud et al.*, 2014] conducted at 30 Hz in natural sandy silt exhibited a 1% drop in velocity (i.e., 2% drop in elastic modulus) at 30 microstrains. Unlike here, the component at 1*f* was larger than the 0*f* component, leading up to −6% in elastic modulus during dilation phases. On the other hand, increasing pressure with depth (≃25 MPa/km) is expected to reduce such nonlinear effects, as seen in Figure 3b where nonlinearity drops by an order of magnitude over the pressure range (0–30 MPa). Additional data would be needed to see if nonlinearity keeps dropping at larger pressures (P_c >30 MPa) or if it reaches a plateau. Nonetheless, nonlinearity is generally orders of magnitude larger in unconsolidated materials [*Johnson and Jia*, 2005; *Brunet et al.*, 2008; *Renaud et al.*, 2014] than in intact rocks. Further, the presence of large fluid pressure at depth can maintain large nonlinear effects by lowering effective stresses. Therefore, we argue that nonlinearity (and the softening phenomenon in particular) may be present in the Earth's crust, particularly near fault zones where highly cracked rocks/unconsolidated gouge is present and within sediment basins where trapped waves lead to strong ground shaking. Finally, this (nonlinear) elastic softening leads to liquefaction phenomena [*Frankel et al.*, 2002; *Zeghal and Elgamal*, 1994; *Zeghal et al.*, 1995], when pore pressure within saturated soils increases due to strong ground motion, leading to large drops in effective stresses.

5. Conclusions

This study aims at characterizing the frequency and pressure dependences of nonlinear elasticity in a sample of room dry Berea sandstone. As previously observed with quasi-static tests and resonance techniques [*TenCate*, 2011], we find that nonlinearity increases with frequency. Nonlinearity increases by a factor 2 or 3 over 3 orders of magnitude in frequency (0.2 to 200 Hz). In addition, we find that not all nonlinear components increase with frequency: only the components at 0*f*, 2*f*, 4*f*, and 6*f* do so. In comparison, the component at 1*f* appears rather frequency independent. (Note that the components at 0*f*, 2*f*, 4*f*, and 6*f* for such pump-probe scheme are equivalent to *odd* harmonics in standard nonlinear acoustic techniques (when the probing wave also acts as a pump), whereas the component at 1*f* is equivalent to the second harmonic). This result indicates that nonlinear elasticity in rocks does depend on the strain rate and not only on the sign of strain rate as described by previous nonlinear elastic theories [*McCall and Guyer*, 1994]. This result also confirms that nonlinear elastic components can be divided into two categories [*Rivière et al.*, 2015], likely arising from two main mechanisms: one related to the component at 1*f* and the other related to the components at 0*f*, 2*f*, 4*f*, 6*f*, etc. In addition, we find that all nonlinear components decrease exponentially with confining pressures, with characteristic pressures around 10 MPa for this room dry Berea sample (Figure 3 and Table 1).

The relative small change in nonlinear response with frequency (factor 2 or 3 over 3 orders of magnitude in frequency) suggests that phenomena observed at the laboratory scale with acoustic experiments (kHz range) are likely to occur in the Earth at seismic frequencies. In particular, the component at 0*f* corresponds to a transient elastic softening of the medium during small (micro)strain dynamic perturbations. Such transient softening has indeed been observed in small scale field experiments [*Johnson et al.*, 2009; *Renaud et al.*, 2014] and in the upper crust following earthquakes [e.g., *Rubinstein et al.*, 2007; *Rubinstein and Beroza*, 2005; *Wu et al.*, 2009; *Rubinstein*, 2011; *Brenguier et al.*, 2008]. It has also been observed due to Earth tidal oscillations (implying strain lower than 0.1 microstrain) by *Hillers et al.* [2015].

Experiments with more (diverse) rock samples, and under more diverse conditions of temperature, humidity and saturation, will be carried out in future work to further characterize the link between nonlinear elasticity and rock microstructure, with the goal of developing a unified physics-based theory, as well as improving our interpretation of crustal's scale observations.

Acknowledgments

This material is based upon work supported by the U.S. Department of Energy, Office of Science, Office of Basic Energy Sciences, Chemical Sciences, Geosciences, and Biosciences Division. Data are available upon request by contacting J. Rivière (jvr5626@psu.edu).

References

Aguirre, J., and K. Irikura (1997), Nonlinearity, liquefaction, and velocity variation of soft soil layers in Port Island, Kobe, during the Hyogo-Ken Nanbu earthquake, *Bull. Seismol. Soc. Am.*, *87*(5), 1244–1258.

Aleshin, V., and K. E. A. Van Den Abeele (2007a), Friction in unconforming grain contacts as a mechanism for tensorial stress-strain hysteresis, *J. Mech. Phys. Solids*, *55*(4), 765–787.

Aleshin, V., and K. E. A. Van Den Abeele (2007b), Microcontact-based theory for acoustics in microdamaged materials, *J. Mech. Phys. Solids*, *55*, 366–390, doi:10.1016/j.jmps.2006.07.002.

Batzle, M. L., D.-H. Han, and R. Hofmann (2006), Fluid mobility and frequency-dependent seismic velocity—Direct measurements, *Geophysics*, *71*(1), N1–N9.
Beresnev, I. A., and K.-L. Wen (1996), Nonlinear soil response—A reality?, *Bull. Seismol. Soc. Am.*, *86*(6), 1964–1978.
Brace, W., J. Walsh, and W. Frangos (1968), Permeability of granite under high pressure, *J. Geophys. Res.*, *73*(6), 2225–2236.
Brenguier, F., M. Campillo, C. Hadziioannou, N. Shapiro, R. Nadeau, and E. Larose (2008), Postseismic relaxation along the San Andreas fault at Parkfield from continuous seismological observations, *Science*, *321*(5895), 1478–1481.
Brunet, T., X. Jia, and P. Johnson (2008), Transitional nonlinear elastic behaviour in dense granular media, *Geophys. Res. Lett.*, *35*, L19308, doi:10.1029/2008GL035264.
Bruno, C., A. Gliozzi, M. Scalerandi, and P. Antonaci (2009), Analysis of elastic nonlinearity using the scaling subtraction method, *Phys. Rev. B*, *79*(6), 64108.
Buck, O., W. Morris, and J. Richardson (1978), Acoustic harmonic generation at unbonded interfaces and fatigue cracks, *Appl. Phys. Lett.*, *33*, 371–373.
Favrie, N., B. Lombard, and C. Payan (2015), Fast and slow dynamics in a nonlinear elastic bar excited by longitudinal vibrations, *Wave Motion*, *56*, 221–238.
Field, E., P. Johnson, I. Beresnev, and Y. Zeng (1997), Nonlinear ground-motion amplification by sediments during the 1994 Northridge earthquake, *Nature*, *390*(6660), 599–602.
Fortin, J., A. Schubnel, and Y. Guéguen (2005), Elastic wave velocities and permeability evolution during compaction of bleurswiller sandstone, *Int. J. Rock Mech. Mining Sci.*, *42*(7–8), 873–889.
Frankel, A. D., D. L. Carver, and R. A. Williams (2002), Nonlinear and linear site response and basin effects in Seattle for the M 6.8 Nisqually, Washington, earthquake, *Bull. Seismol. Soc. Am.*, *92*(6), 2090–2109.
Gliozzi, A., and M. Scalerandi (2014), Modeling dynamic acousto-elastic testing experiments: Validation and perspectives, *J. Acoust. Soc. Am.*, *136*(4), 1530–1541.
Gusev, V., and V. Tournat (2005), Amplitude- and frequency-dependent nonlinearities in the presence of thermally-induced transitions in the preisach model of acoustic hysteresis, *Phys. Rev. B*, *72*(5), 54104.
Guyer, R., and P. Johnson (2009), *Nonlinear Mesoscopic Elasticity: The Complex Behaviour of Rocks, Soil, Concrete*, 395 pp., Wiley Vch Publ., Hoboken, N. J.
Guyer, R. A., K. R. McCall, G. N. Boitnott, L. B. Hilbert, and T. J. Plona (1997), Quantitative implementation of preisach-mayergoyz space to find static and dynamic elastic moduli in rock, *J. Geophys. Res.*, *102*, 5281–5293.
Hillers, G., L. Retailleau, M. Campillo, A. Inbal, J.-P. Ampuero, and T. Nishimura (2015), In situ observations of velocity changes in response to tidal deformation from analysis of the high-frequency ambient wavefield, *J. Geophys. Res. Solid Earth*, *120*, 210–225, doi:10.1002/2014JB011318.
Johnson, P. A., and X. Jia (2005), Nonlinear dynamics, granular media and dynamic earthquake triggering, *Nature*, *437*(7060), 871–874.
Johnson, P. A., P. Bodin, J. Gomberg, F. Pearce, Z. Lawrence, and F.-Y. Menq (2009), Inducing in situ, nonlinear soil response applying an active source, *J. Geophys. Res.*, *114*, B05304, doi:10.1029/2008JB005832.
Kaselow, A., and S. A. Shapiro (2004), Stress sensitivity of elastic moduli and electrical resistivity in porous rocks, *J. Geophys. and Eng.*, *1*(1), 1–11.
Lawn, B. R., and D. B. Marshall (1998), Nonlinear stress-strain curves for solids containing closed cracks with friction, *J. Mech. Phys. Solids*, *46*(1), 85–113.
Lebedev, A., and L. Ostrovsky (2014), A unified model of hysteresis and long-time relaxation in heterogeneous materials, *Acoust. Phys.*, *60*(5), 555–561.
McCall, K., and R. Guyer (1994), Equation of state and wave-propagation in hysteretic nonlinear elastic-materials, *J. Geophys. Res.*, *99*, 23,887–23,897.
Moreschi, H., S. Callé, S. Guerard, D. Mitton, G. Renaud, and M. Defontaine (2011), Monitoring trabecular bone microdamage using a dynamic acousto-elastic testing method, *Proc. Inst. Mech. Eng.*, *225*(3), 282–295.
Nihei, K., L. Hilbert Jr., N. Cook, S. Nakagawa, and L. Myer (2000), Frictional effects on the volumetric strain of sandstone, *Int. J. Rock Mech. Min. Sci.*, *37*(1), 121–132.
Ougier-Simonin, A., Y. Guéguen, J. Fortin, A. Schubnel, and F. Bouyer (2011), Permeability and elastic properties of cracked glass under pressure, *J. Geophys. Res.*, *116*, B07203, doi:10.1029/2010JB008077.
Pecorari, C. (2015), A constitutive relationship for mechanical hysteresis of sandstone materials, *Proc. R. Soc. A*, *471*, 20150369, doi:10.1098/rspa.2015.0369.
Pimienta, L., J. Fortin, and Y. Guéguen (2015a), Bulk modulus dispersion and attenuation in sandstones, *Geophysics*, *80*(2), D111–D127.
Pimienta, L., J. Fortin, and Y. Guéguen (2015b), Young modulus dispersion and attenuation in sandstones, *Geophysics*, *80*(5), L57–L72.
Renaud, G., S. Callé, and M. Defontaine (2009), Remote dynamic acoustoelastic testing: Elastic and dissipative acoustic nonlinearities measured under hydrostatic tension and compression, *Appl. Phys. Lett.*, *94*, 11905, doi:10.1063/1.3064137.
Renaud, G., S. Callé, and M. Defontaine (2010), Dynamic acoustoelastic testing of weakly pre-loaded unconsolidated water-saturated glass beads, *J. Acoust. Soc. Am.*, *128*, 3344.
Renaud, G., M. Talmant, S. Callé, M. Defontaine, and P. Laugier (2011), Nonlinear elastodynamics in micro-inhomogeneous solids observed by head-wave based dynamic acoustoelastic testing, *J. Acoust. Soc. Am.*, *130*(6), 3583–3589.
Renaud, G., J. Rivière, S. Haupert, and P. Laugier (2013a), Anisotropy of dynamic acoustoelasticity in limestone, influence of conditioning, and comparison with nonlinear resonance spectroscopy, *J. Acoust. Soc. Am.*, *133*, 3706–3718.
Renaud, G., J. Rivière, P. Le Bas, and P. Johnson (2013b), Hysteretic nonlinear elasticity of Berea sandstone at low vibrational strain revealed dy dynamic acousto-elastic testing, *Geophys. Res. Lett.*, *40*(4), 715–719.
Renaud, G., J. Rivière, C. Larmat, J. Rutledge, R. Lee, R. Guyer, K. Stokoe, and P. Johnson (2014), In situ characterization of shallow elastic nonlinear parameters with dynamic acoustoelastic testing, *J. Geophys. Res. Solid Earth*, *119*, 6907–6923, doi:10.1002/2013JB010625.
Rivière, J., G. Renaud, R. Guyer, and P. Johnson (2013), Pump and probe waves in dynamic acousto-elasticity: Comprehensive description and comparison with nonlinear elastic theories, *J. Appl. Phys.*, *114*, 54905.
Rivière, J., P. Shokouhi, R. Guyer, and P. Johnson (2015), A set of measures for the systematic classification of the nonlinear elastic behavior of disparate rocks, *J. Geophys. Res. Solid Earth*, *120*, 1587–1604, doi:10.1002/2014JB011718.
Rubinstein, J. (2011), Nonlinear site response in medium magnitude earthquakes near Parkfield, California, *Bull. Seismol. Soc. Am.*, *101*(1), 275–286.
Rubinstein, J., and G. C. Beroza (2005), Depth constraints on nonlinear strong ground motion from the 2004 Parkfield earthquake, *Geophys. Res. Lett.*, *32*, L14313, doi:10.1029/2005GL023189.

Rubinstein, J., N. Uchida, and G. Beroza (2007), Seismic velocity reductions caused by the 2003 Tokachi-Oki earthquake, *J. Geophys. Res.*, *112*, B05315, doi:10.1029/2006JB004440.
Sayers, C. (2002), Stress-dependent elastic anisotropy of sandstones, *Geophys. Prospect.*, *50*(1), 85–95.
Scalerandi, M., S. Idjimarene, M. Bentahar, and R. El Guerjouma (2015), Evidence of microstructure evolution in solid elastic media based on a power law analysis, *Comm. Nonlin. Sci. Num. Sim.*, *22*(1), 334–347.
TenCate, J. (2011), Slow dynamics of earth materials: An experimental overview, *Pure Appl. Geophys.*, *168*(12), 2211–2219.
TenCate, J., and T. Shankland (1996), Slow dynamics in the nonlinear elastic response of Berea sandstone, *Geophys. Res. Lett.*, *23*, 3019–3022.
Tournat, V., C. Inserra, and V. Gusev (2008), Non-cascade frequency-mixing processes for elastic waves in unconsolidated granular materials, *Ultrasonics*, *48*(6–7), 492–497.
Trarieux, C., S. Callé, H. Moreschi, G. Renaud, and M. Defontaine (2014), Modeling nonlinear viscoelasticity in dynamic acoustoelasticity, *Appl. Phys. Lett.*, *105*(26), 264103.
Trifunac, M., and M. Todorovska (1996), Nonlinear soil response—1994 Northridge, California, earthquake, *J. Geotech. Eng.*, *122*(9), 725–735.
Tutuncu, A., A. Podio, and M. Sharma (1998), Nonlinear viscoelastic behavior of sedimentary rocks, Part II: Hysteresis effects and influence of type of fluid on elastic moduli, *Geophysics*, *63*(1), 195–203.
Vakhnenko, O., V. Vakhnenko, and T. Shankland (2005), Soft-ratchet modeling of end-point memory in the nonlinear resonant response of sedimentary rocks, *Phys. Rev. B*, *71*, 174103.
Van Den Abeele, K. E.-A., P. Johnson, R. Guyer, and K. McCall (1997), On the quasi-analytic treatment of hysteretic nonlinear response in elastic wave propagation, *J. Acoust. Soc. Am.*, *101*, 1885–1898.
Van Den Abeele, K. E.-A., J. Carmeliet, J. Ten Cate, and P. Johnson (2000), Nonlinear elastic wave spectroscopy (news) techniques to discern material damage, Part II: Single-mode nonlinear resonance acoustic spectroscopy, *Res. Nondestr. Eval.*, *12*, 31–42.
Wang, X.-Q., A. Schubnel, J. Fortin, Y. Guéguen, and H.-K. Ge (2013), Physical properties and brittle strength of thermally cracked granite under confinement, *J. Geophys. Res. Solid Earth*, *118*, 6099–6112, doi:10.1002/2013JB010340.
Winkler, K., and X. Liu (1996), Measurements of third-order elastic constants in rocks, *J. Acoust. Soc. Am.*, *100*(3), 1392–1398.
Winkler, K., and L. McGowan (2004), Nonlinear acoustoelastic constants of dry and saturated rocks, *J. Geophys. Res.*, *109*, B10204, doi:10.1029/2004JB003262.
Wu, C., Z. Peng, and Y. Ben-Zion (2009), Non-linearity and temporal changes of fault zone site response associated with strong ground motion, *Geoph. J. Int.*, *176*(1), 265–278.
Zeghal, M., and A.-W. Elgamal (1994), Analysis of site liquefaction using earthquake records, *J. Geotech. Eng.*, *120*(6), 996–1017.
Zeghal, M., A.-W. Elgamal, H. Tang, and J. Stepp (1995), Lotung downhole array. II: Evaluation of soil nonlinear properties, *J. Geotech. Eng.*, *121*(4), 363–378.
Zimmerman, R., W. Somerton, and M. King (1986), Compressibility of porous rocks, *J. Geophys. Res.*, *91*(B12), 12,765–12,777.
Zinszner, B., P. A. Johnson, and P. N. J. Rasolofosaon (1997), Influence of change in physical state on elastic nonlinear response in rock: Significance of effective pressure and water saturation, *J. Geophys. Res.*, *102*, 8105–8120.